

Injectable Anti-inflammatory Nanofiber Hydrogel to Achieve Systemic Immunotherapy Post Local Administration

Muchao Chen, Yanjun Tan, Ziliang Dong, Jiaqi Lu, Xiao Han, Qiutong Jin, Wenjun Zhu, Jingjing Shen, Liang Cheng, Zhuang Liu,* and Qian Chen*



Cite This: <https://dx.doi.org/10.1021/acs.nanolett.0c02684>



Read Online

ACCESS |

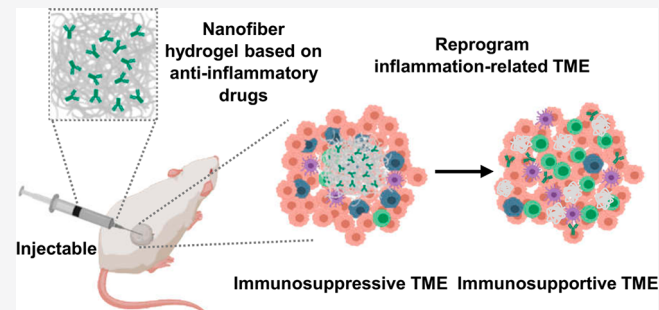
Metrics & More

Article Recommendations

Supporting Information

ABSTRACT: Despite the great promise achieved by immune checkpoint blockade (ICB) therapy in harnessing the immune system to combat different tumors, limitations such as low objective response rates and adverse effects remain to be resolved. Here, an anti-inflammatory nanofiber hydrogel self-assembled by steroid drugs is developed for local delivery of antiprogrammed cell death protein ligand 1 (α PDL1). Interestingly, on the one hand this carrier-free system based on steroid drugs can reprogram the pro-tumoral immunosuppressive tumor microenvironment (TME) to antitumoral TME; on the other hand, it would serve as a reservoir for sustained release of α PDL1 so as to synergistically boost the immune system. By local injection of such α PDL1-loaded hydrogel, effective therapeutic effects were observed in inhibiting both local tumors and abscopal tumors without any treatment. This work presents a unique hydrogel-based delivery system using clinically approved drugs, showing promise in improving the objective response rate of ICB therapy and minimizing its systemic toxicity.

KEYWORDS: *nanofiber hydrogel, anti-inflammatory, steroid drugs, immune checkpoint blockade, cancer immunotherapy*



Immune checkpoint blockade (ICB) therapy, which usually prevents T cell anergy, apoptosis, and exhaustion, has gained prominence owing to the satisfactory clinical efficacy in various malignancies.^{1–3} In particular, blocking the interaction between programmed death-1 (PD-1) and programmed death-ligand 1 (PD-L1) with antibodies could restore T cell functions and activate strong antitumor immune responses.^{4,5} However, only a relatively small fraction of patients would show responses to ICB because of the high interstitial fluid pressure, the low infiltration of T cells, and the presence of large numbers of immunosuppressive cells including regulatory T cells (Tregs), myeloid-derived suppressor cells (MDSCs) in the tumor microenvironment (TME).^{6–8} Moreover, systemic administration of ICB inhibitors may induce various immune-related side effects associated with the overactivation of the immune system.^{9–11} Thus, efforts focused on increasing the response rate of ICB (e.g., by reprogramming the immunosuppressive TME), and avoiding the adverse effect of ICB antibodies remain an important issue in the field of cancer immunotherapy.^{6,12–14}

Inflammation has been reported as an important factor in TME to promote tumor development.^{15–17} Such tumor-associated inflammation is featured with the presence of innate immune cells including different subtypes of neutrophils, mast cells, dendritic cells (DCs) and MDSCs, adaptive immune cells such as T lymphocytes, as well as the surrounding stroma

containing endothelial cells, fibroblasts, and pericytes.^{8,18,19} The communication in diverse cell types, the expression of various immune modulators, and mediators together with the activation state of different cells in TME are closely related to the balance between anti-tumor immunity and pro-tumor inflammation.^{20–22} In established tumors, this balance tends to pro-tumor inflammation and promotes tumor growth.^{20,23} In line with these, the immunosuppressive TME associated with pro-tumor inflammation in solid tumors usually would lead to their poor responses to ICB therapy.^{24–25} Thus, reprogramming the chronic pro-tumor inflammatory microenvironment is likely to liberate and activate the existing effective antitumor T cells and may be a promising strategy to promote the antitumor immune responses and increase the ICB responsive rate.^{26–28}

Hydrogels, a promising type of “intelligent” drug delivery system, allow controlled and sustained release of different bioactive agents.²⁹ Typically, nanofiber hydrogels, which are formed by cross-linking of filamentous assemblies via physical

Received: June 29, 2020

Revised: July 30, 2020

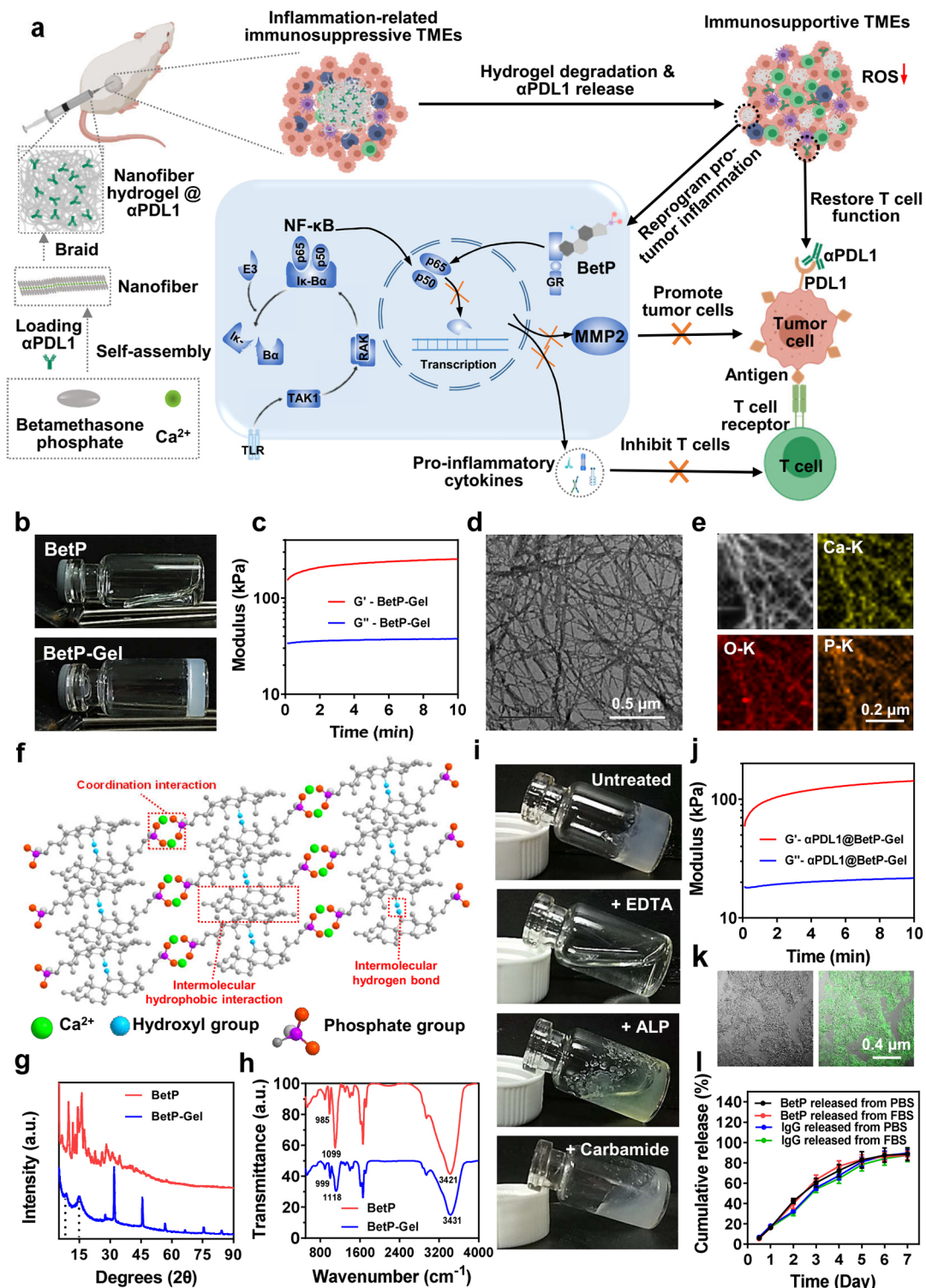


Figure 1. The formation and characterization of nanofiber anti-inflammatory hydrogel. (a) Schematic shows the formation of nanofiber hydrogel by cross-linking filamentous assemblies via physical interaction between betamethasone phosphate and calcium ion. Such nanofiber hydrogel composed by anti-inflammatory steroid on the one hand could reprogram the pro-tumoral immunosuppressive TME to anti-tumoral TME via inhibiting NF-κB signal pathway, and on the other hand could sustainably release αPDL1 to activate T cells, so as to synergistically boost the immune attack of tumor cells. (b) Photographs showing BetP solution (without addition of Ca²⁺) and hydrogel (with addition of Ca²⁺). (c) Rheological behavior of BetP hydrogel. G' , storage modulus; G'' , loss modulus. (d) Representative TEM image of BetP hydrogel. (e) Representative element mapping images of BetP hydrogel. (f) Ball-and-stick model of BetP nanofiber hydrogel showing the intermolecular noncovalent interactions, including coordination interactions, hydrophobic interactions, and hydrogen bonds. (g) XRD patterns of BetP powder and BetP hydrogel. a.u., arbitrary unit. (h) FTIR spectra of BetP powder and BetP hydrogel. (i) Photographs of BetP hydrogel alone, or with addition of EDTA (50 mM), ALP (1 μM), and carbamide (1 M). (j) Rheological behavior of BetP hydrogel encapsulated with αPDL1. G' , storage modulus; G'' , loss modulus. (k) Representative fluorescent images of BetP hydrogel encapsulated with αPDL1 in which αPDL1 was stained with Alexa Fluor 488-conjugated antimouse antibody (left, bright field image; right, fluorescence image). (l) Cumulative release profiles of BetP and IgG

Figure 1. continued

from BetP hydrogel in PBS or PBS + 10% FBS for 7 days in 37 °C. Experiments were repeated three times. Data are presented as mean ± s.e.m. ($n = 3$).

interaction, exhibit reparable gel–sol phase transition, allowing their direct injection into the tissue with minimal invasiveness.^{30–35} Designing therapeutic drugs as effective hydrogelator to create “self-delivery” nanofiber hydrogel has attracted wide attention.^{36,37} According to previous reports,³⁸ many steroid drugs (such as betamethasone phosphate, dexamethasone phosphate, and hydrocortisone phosphate) with a rigid hydrophobic core composed of four fused rings, a phosphate group, and several hydroxyl groups, could form nanofiber hydrogels via different interactions. Herein, we develop a shear-thinning injectable nanofiber hydrogel based on betamethasone phosphate, a widely used anti-inflammatory steroid drug for arthritis and asthma treatment in clinic,^{39,40} to enable effective reprogramming of immunosuppressive TME and sustained release of PDL1 antibody (α PDL1) for enhanced cancer immunotherapy (Figure 1a). Such nanofiber hydrogel is formed by noncovalent interactions including intermolecular hydrogen bonds and hydrophobic interactions between steroid molecules, as well as coordination between phosphate groups and calcium ions, permitting its direct injection into the tissues with minimal invasiveness. This anti-inflammatory steroid drug-based nanofiber hydrogel itself could reprogram the inflammation-related immunosuppressive TME including improving the tumor infiltration of effective T lymphocytes and reducing the percentages of immunosuppressive cells. Moreover, this nanofiber hydrogel also served as an effective reservoir for controlled and sustained release of α PDL1 to boost the T cell mediated immune responses to attack cancer cells, significantly inhibiting the local tumor growth. Interestingly, strong abscopal effect of such nanofiber hydrogel was also observed on mice with distant tumors.

The betamethasone phosphate hydrogel (BetP-Gel) was formed promptly by mixing betamethasone phosphate disodium (BetP) solution and calcium chloride (CaCl_2) aqueous solution (Figure 1a and Supporting Information Figure S1). The macroscopic sol–gel transition was observed clearly, and the formed complex exhibited typical hydrogel characteristics such as maintainable integrity and shape (remaining in a slant bottle) (Figure 1b). The lowest gelation concentration of BetP was about 0.01 M as reflected in the formation of self-supporting hydrogel with different concentrations of BetP (Figure S2). The formation of BetP-Gel was further confirmed by rheological behavior test (Figure 1c). The value of storage modulus (G') was much higher than that of loss modulus (G''), indicating a representative elastic network in BetP-Gel (0.05 M). Moreover, the BetP-Gel with extended nanofiber network was also observed in transmission electron microscope (TEM) imaging (Figure 1d). The elemental mapping further indicated the uniform distribution of BetP and calcium ion in the network structure (Figure 1e). Interestingly, as shown in the SI Video, the nanofiber hydrogel could rapidly recover (self-healing) after being injected from a syringe (shear-thinning). This fast recovery rate could prevent sedimentation or leakage of encapsulated therapeutic drugs during the injection process. As expected, the integrated and mechanical properties of this hydrogel were maintained after injection as exhibited in Figure S3a–c.

We hypothesized that the nanofiber hydrogels with filamentous structures were formed by various noncovalent interactions including the coordination interactions between phosphate groups in BetP and calcium ions (Ca^{2+}), the intermolecular hydrogen bonds between hydroxyl groups in BetP, and the intermolecular hydrophobic interactions between rigid steroid nuclei in BetP (Figure 1f). To verify our hypothesis, we investigated the BetP powder and freeze-dried BetP-Gel with X-ray diffraction (XRD) and Fourier transform infrared spectroscopy (FTIR). As shown in the XRD pattern, BetP displayed typical crystalline properties with specific reflections in the range of 5–45°. These diffuse scattering peaks at 7.0° and 15.0° might be associated with the amorphous state of BetP– Ca^{2+} complex, and the other peaks were a typical crystal reflection of sodium chloride (byproduct in hydrogel) (Figure S4), indicating the coordination interactions between phosphate group and Ca^{2+} during the hydrogelation process (Figure 1g). FTIR data showed that the specific bands (985 and 1099 cm^{-1}) for the phosphate group shifted to higher wavenumbers (999 and 1118 cm^{-1}), further indicating the coordination bonds between phosphate groups and Ca^{2+} (Figure 1h). Moreover, the coordination interactions between phosphate group and Ca^{2+} were further verified by incubating BetP-Gel with ethylene diamine tetraacetic acid (EDTA, a chelator for Ca^{2+}) or alkaline phosphatase (ALP, a scissor for phosphate groups), which resulted in the transformation of BetP-Gel into solutions (Figure 1i). In addition, the hydroxyl groups vibration band in BetP at 3421 cm^{-1} was shifted to 3431 cm^{-1} , indicating stronger hydrogen bonds in the formed BetP-Gel (Figure 1h), which was further verified by the microscopical gel–sol transition after incubation with carbamide (a competing agent for hydrogen bond) (Figure 1i). Similar to bile acid derivatives, which can form nanofiber hydrogel via intermolecular hydrophobic interactions, BetP molecules with rigid steroid nuclei may also form intermolecular hydrophobic interactions between steroid nuclei structures during the self-assembly process.^{41–43} Therefore, the coordinations between Ca^{2+} and phosphate groups, as well as the intermolecular hydrogen bonds and hydrophobic interactions, all together contribute to the formation of BetP-Gel.

Inspired by the quick sol–gel translation as well as shear-thinning and self-healing ability of BetP-Gel, it could be used to deliver α PDL1 by simply mixing BetP solution containing antibodies with CaCl_2 solution. To prepare α PDL1 encapsulated BetP hydrogel, α PDL1 at the therapeutic dose was loaded into the BetP-Gel. The α PDL1-loaded hydrogel exhibited similar rheology properties to BetP-Gel, indicating that the encapsulation of antibodies did not obviously affect the formation of hydrogel (Figure 1j). As visualized by confocal imaging of the frozen sections of hydrogel stained with goat antimouse IgG H&L (Alexa Fluor 488) antibody, α PDL1 showed uniform distribution in the formed α PDL1@BetP-Gel (Figure 1k). Furthermore, thanks to the competitive interaction between phosphate in physiological conditions and Ca^{2+} ions in the hydrogel, BetP-Gel could be gradually degraded to release the encapsulated antibodies. In phosphate buffered saline (PBS) and fetal bovine serum (FBS), BetP-Gel

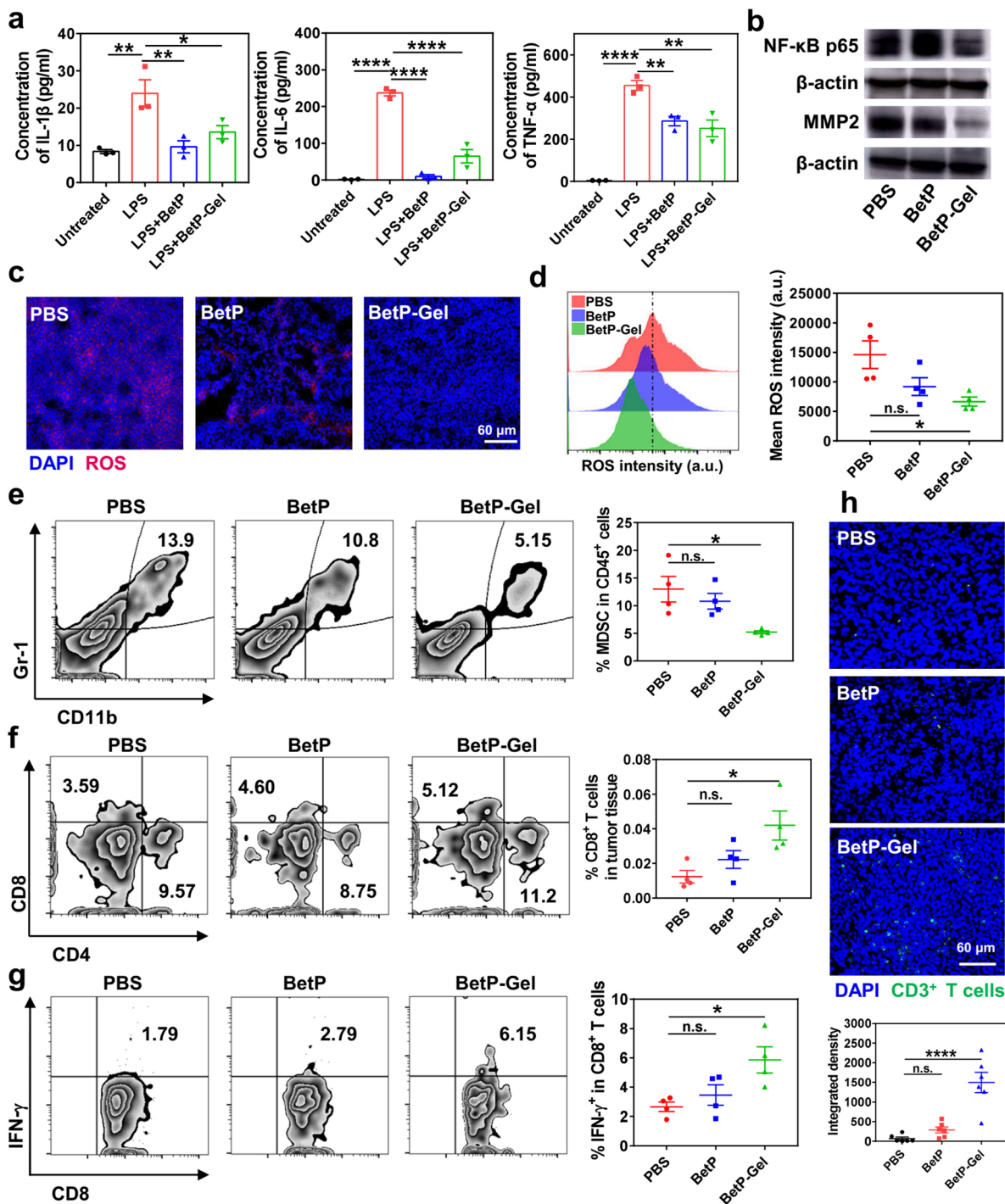


Figure 2. Anti-inflammatory immune responses induced by the nanofiber hydrogel based on steroid drug. (a) Secretion levels of pro-inflammatory cytokines (IL-1 β , IL-6, TNF- α) by BMDMs. Data are presented as mean \pm s.e.m. ($n = 3$). (b) The level of inflammation-related proteins (NF-κB p65 and MMP2) in the tumor analyzed by Western blotting. Experiments were repeated three times. (c,d) ROS levels in the tumor were measured using CellROX Oxidative Stress Reagents by (c) confocal fluorescence imaging and (d) flow cytometric analyses. a.u., arbitrary unit. Data are presented as mean \pm s.e.m. ($n = 4$). (e) Percentages of murine MDSCs (CD45 $^{+}$ CD11b $^{+}$ Gr-1 $^{-}$) in the tumor analyzed by flow cytometry. Data are presented as mean \pm s.e.m. ($n = 4$). (f) Percentages of CD8 $^{+}$ TILs (CD3 $^{+}$ CD8 $^{+}$) in the tumor analyzed by flow cytometry. Data are presented as mean \pm s.e.m. ($n = 4$). (g) Percentages of IFN- γ positive CD8 $^{+}$ TILs (CD3 $^{+}$ CD8 $^{+}$ IFN- γ $^{+}$) in the tumor analyzed by flow cytometry. Data are presented as mean \pm s.e.m. ($n = 4$). (h) Representative immunofluorescence images showing CD3 $^{+}$ T cells infiltrated in the tumor. Data are presented as mean \pm s.e.m. ($n = 6$). Statistical significance was calculated via one-way ANOVA with a Tukey posthoc test. * $P < 0.05$; ** $P < 0.01$; *** $P < 0.001$; **** $P < 0.0001$.

could be degraded and sustainably release 90% of the encapsulated antibodies within 7 days (Figure S5 and Figure 11).

The chronic inflammation elevated during tumor development is closely related to the immunosuppressive TME at different stages of the tumor, increasing the potential of tumor

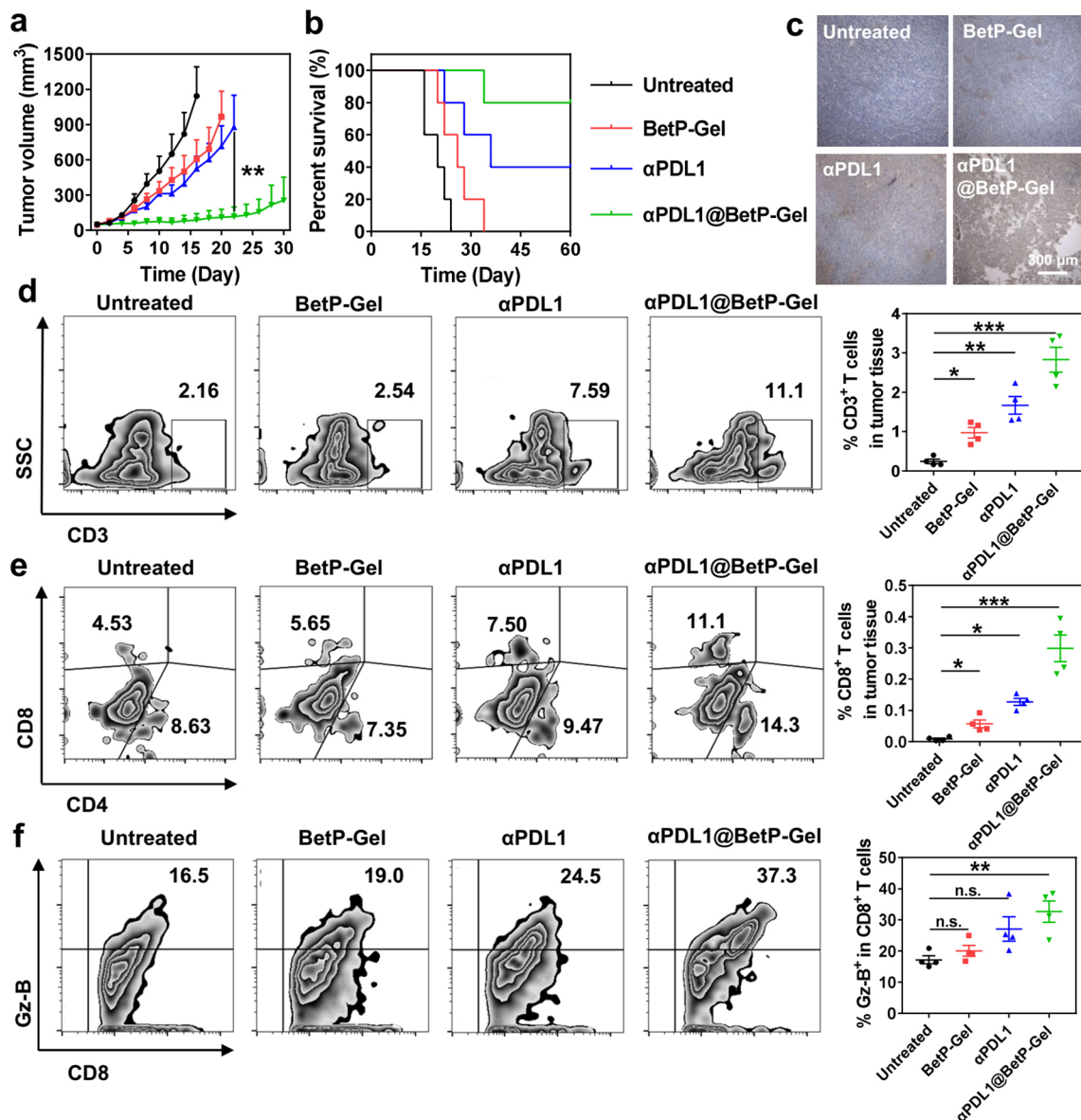


Figure 3. $\alpha\text{PDL1@BetP-Gel}$ triggering the robust antitumor immune responses. (a) Tumor growth kinetics in different groups. Growth curves were stopped when the first mouse in the corresponding group died. Data are presented as mean \pm s.e.m. ($n = 5$). (b) Survival corresponding to the tumor size of mice in different groups. (c) Micrographs of TUNEL stained tumor slices collected from mice in different groups at 48 h. (d) Percentages of TILs (CD3⁺) in the tumor analyzed by flow cytometry. Data are presented as mean \pm s.e.m. ($n = 4$). (e) Percentages of CD8⁺ TILs (CD3⁺CD8⁺) in the tumor analyzed by flow cytometry. Data are presented as mean \pm s.e.m. ($n = 4$). (f) Percentages of Gz-B positive CD8⁺ TILs (CD3⁺CD8⁺Gz-B⁺) in the tumor analyzed by flow cytometry. Data are presented as mean \pm s.e.m. ($n = 4$). Statistical significance was calculated via one-way ANOVA with a Tukey posthoc test. * $P < 0.05$; ** $P < 0.01$; *** $P < 0.001$.

invasion and migration.^{15,44,45} Considering that the steroid drug, BetP, is a widely used anti-inflammatory agent,⁴⁶ we investigated the changes of inflammation and immune responses after BetP-Gel treatment. We first evaluated the anti-inflammatory effect of BetP-Gel in the bone marrow derived macrophages (BMDMs)-cell level. Specifically, BMDMs were incubated in the presence of a strong immune stimulus, lipopolysaccharide (LPS), which induced the significant secretion of pro-inflammatory cytokines such as IL-1 β , IL-6, IL-12p70, and TNF- α by BMDMs. Interestingly, the addition of free BetP or BetP-Gel could effectively eliminate the generation of inflammatory cytokines (Figure 2a and Figure S6).

According to previous literature, BetP, as a typical glucocorticoid, could attenuate inflammation-related nuclear factor kappa-B (NF- κ B) signaling pathway and suppress the genetic transcription of pro-inflammatory cytokines and matrix metalloproteinase (MMP2), when it integrates with glucocorticoid receptor (GR) in cytoplasm.^{47–49} Different from the molecular mechanism of noncanonical NF- κ B pathway,^{50,51} BetP could inhibit canonical NF- κ B pathway by interfering NF- κ B p65 translocation to the nucleus and decrease MMP2-related transcription to reprogram tumor-promoting chronic inflammation.^{52,53} According to previously published work, MMP2 is an important downstream signal channel of NF- κ B related to the immune system, which plays a key role in inhibiting the adaptive immune responses.^{54,55} For example,

MMP2 could cleave different growth factors and cytokine receptors, such as IL-2 receptor ($\text{IL-2}\alpha$), and thereby inhibit the proliferation and activation of T cells. Thus, inhibiting the expression and activity of MMP2 has the potential to reprogram the pro-tumor inflammation-related TME.^{49,56–59} First, we investigated the expression of inflammation-related proteins, NF- κB p65 and MMP2, in the TME after different treatments using Western blotting. In our experiments, Balb/c mice bearing CT26 murine colon tumors were intratumorally injected with PBS, free BetP, or BetP-Gel. Remarkably, compared to the control and free BetP treated groups (puny effect due to the short retention in the tumor), BetP-Gel injection significantly downregulated the expression of both NF- κB p65 and MMP2 in the tumor (Figure 2b, Figure S7a–f, and Figure S8a,b). We further studied the levels of inflammation-related reactive oxygen species (ROS) in the TME after free BetP or BetP-Gel treatment. As shown in the confocal imaging (Figure 2c and Figure S9) and flow cytometry analysis (Figure 2d), the ROS levels obviously decreased after intratumoral (i.t.) injection of BetP-Gel.

Encouraged by the anti-inflammatory effect of BetP-Gel, we next evaluated different immune cells related to pro-tumor inflammation in the tumor after different treatments. We measured the populations of different immune cells on day 5 after i.t. injection of PBS, BetP, or BetP-Gel. The percentage of immune cells (CD45^+) (Figure S11a) showed increase, and the population of inflammation related MDSCs ($\text{CD45}^+\text{CD11b}^+\text{Gr-1}^+$) (Figure 2e) decreased. Moreover, the frequencies of CD8^+ tumor-infiltrating lymphocytes ($\text{CD3}^+\text{CD8}^+$, TILs) (Figure 2f) and interferon- γ positive CD8^+ TILs ($\text{CD3}^+\text{CD8}^+\text{IFN-}\gamma^+$) (Figure 2g and Figure S10), as well as the percentage of typical antigen-presenting dendritic cells (CD11c^+ , DCs) (Figure S11b) within the tumor obviously increased in BetP-Gel treated group. More interestingly, the immunosuppressive cells, such as regulatory T cells ($\text{CD3}^+\text{CD4}^+\text{FOXP3}^+$, Tregs) showed a slight decrease in population in the tumor after BetP-Gel treatment (Figure S11c). The infiltration of effective T cells was also confirmed by the immunofluorescence staining of CD3^+ TIL cells (Figure 2h). Taken together, local injection of BetP-Gel into the tumor with sustained release of anti-inflammatory drug BetP could down-regulate the inflammation-related ROS level, improve the tumor infiltration of effective TILs, and reduce the percentages of immunosuppressive cells, exhibiting the promising ability in modulating inflammation-related immunosuppressive TME.

To assess the potential of BetP-Gel for in vivo delivery of immunotherapeutics, mice bearing CT26 tumors were i.t. injected with either Cyanine 5.5 labeled αPDL1 (free $\alpha\text{PDL1-Cy5.5}$) or BetP-Gel encapsulating $\alpha\text{PDL1-Cy5.5}$ ($\alpha\text{PDL1-Cy5.5@BetP-Gel}$) and monitored by the in vivo fluorescence imaging system (PerkinElmer IVIS Lumina III) at different time points. It was found that the Cy5.5 signals in the tumor injected with free $\alpha\text{PDL1-Cy5.5}$ became undetectable on day 7, indicating that free antibody could quickly diffuse out of the tumor. In contrast, for $\alpha\text{PDL1-Cy5.5@BetP-Gel}$ treated mice, the fluorescence signals from $\alpha\text{PDL1-Cy5.5}$ maintained at high levels within the tumor for long time, indicating the sustained release of $\alpha\text{PDL1-Cy5.5}$ from the hydrogel. Note that the slight increase of tumor fluorescence signals in the first 3 days might be attributed to the gradual release of $\alpha\text{PDL1-Cy5.5}$ from the hydrogel. On day 7, strong fluorescence signals were still observed throughout the whole tumor for $\alpha\text{PDL1-Cy5.5@BetP-Gel}$.

BetP-Gel treated mice (Figure S12). Confocal imaging of tumor tissue sections further confirmed the greatly prolonged retention of αPDL1 within the tumor when it was encapsulated into the BetP-Gel (Figure S13). Therefore, local delivery of αPDL1 using this nanofiber hydrogel could realize controlled and sustained release of therapeutics in an extended period of time.

Next, the synergistic antitumor effect of $\alpha\text{PDL1@BetP-Gel}$ was evaluated in the subcutaneous colorectal tumor model (CT26). BALB/c mice bearing CT26 tumors were divided into four groups: untreated, BetP-Gel (20 μL , 0.05 M BetP per mouse), free αPDL1 (70 μg per mouse), and $\alpha\text{PDL1@BetP-Gel}$ (20 μL , 0.05 M BetP per mouse; 70 μg αPDL1 per mouse). Compared to the BetP-Gel or free αPDL1 treatment, both of which were not sufficient to control the tumor growth, $\alpha\text{PDL1@BetP-Gel}$ significantly inhibited the growth of tumors and prolonged the survival of mice (Figure 3a,b). The obviously synergistic therapeutic effect of $\alpha\text{PDL1@BetP-Gel}$ treatment was further confirmed by the histological examination (Figure 3c and Figure S14). Compared with the other control groups, apparent histological damages were observed in tumor slices collected from $\alpha\text{PDL1@BetP-Gel}$ treated mice. Furthermore, mouse body weights after different treatments exhibited no obvious difference, indicating that the local treatment with $\alpha\text{PDL1@BetP-Gel}$ induced no obvious acute side effects (Figure S15). Moreover, another two important control groups, the free BetP-Sol + αPDL1 (20 μL , 0.05 M BetP per mouse; 70 μg αPDL1 per mouse) and the drug-free hydrogel (calcium alginate hydrogel) containing αPDL1 ($\alpha\text{PDL1@ALG}$) (20 μL , 10% ALG per mouse; 70 μg αPDL1 per mouse), have been added to evaluate their antitumor efficacy. As shown in Figure S16, drug-free hydrogel ($\alpha\text{PDL1@ALG}$) could slightly inhibit the growth of the tumor due to the existence of immunosuppressive tumor micro-environment such as the tumor-promoting chronic inflammation. Moreover, the growth of the tumor in free BetP-Sol + αPDL1 treated group was only inhibited at the very beginning because of the quick diffusion of αPDL1 .

Then, the immune responses after different treatments were further studied in CT26 tumor model. CT26 tumors were collected and analyzed by flow cytometry at day 5 post various treatments. Compared to the untreated group, the frequency of TILs (CD3^+ cells) was obviously increased after either αPDL1 or $\alpha\text{PDL1@BetP-Gel}$ treatments (Figure 3d and Figure S17). More importantly, the percentage of CD8^+ TILs, especially granzyme B (Gz-B) positive CD8^+ TILs, which could secrete Gz-B to induce the apoptosis of cancer cells via degrading their DNA, was significantly increased in $\alpha\text{PDL1@BetP-Gel}$ treated group, further indicating that the number of effective T cells was remarkably increased after regulating the TME and sustained release of αPDL1 (Figure 3e,f and Figure S10). We also evaluated the secretion of IFN- γ in tumor grinding supernatant via Enzyme-linked immunosorbent assay (ELISA) kit (Figure S18). As expected, the level of IFN- γ remarkably increased in $\alpha\text{PDL1@BetP-Gel}$ treated group, further demonstrating the effective activation of T cells after such treatment.

To investigate whether the local treatment could trigger systemic immune responses, which may be utilized to inhibit tumor metastasis, a bilateral CT26 tumor model was used in our following experiment: a first tumor was inoculated on the right side of each mouse designated as the “primary tumor”, which was injected with $\alpha\text{PDL1@BetP-Gel}$, and the second CT26 tumor was inoculated on the left side of mice designated

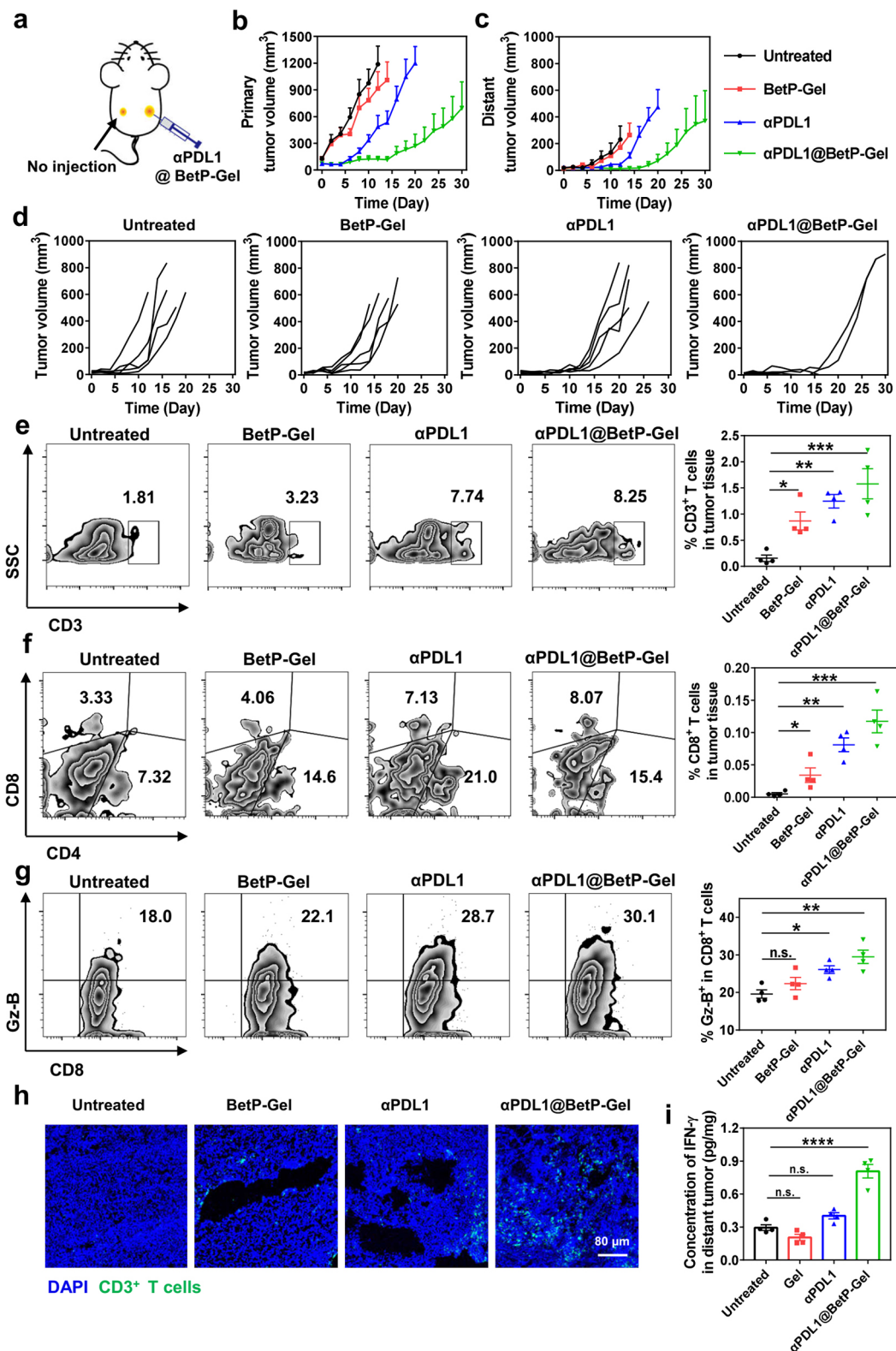


Figure 4. The systemic immune responses induced by local injection of αPDL1 @BetP-Gel. (a) Schematic illustrating the local injection of αPDL1 @BetP-Gel only into the primary tumor. Tumors on the right side were designated as primary tumors with αPDL1 @BetP-Gel injection, and those on the left sides were designated as distant tumors without any treatment. (b) Primary tumor and (c) distant tumor growth kinetics in different groups. Growth curves were stopped when the first mouse in the corresponding group died. Data are presented as mean \pm s.e.m. ($n = 5$). (d) Individual distant tumor growth kinetics in different groups. (e) Percentages of TILs (CD3⁺) in the distant tumors analyzed by flow cytometry. Data are presented as mean \pm s.e.m. ($n = 4$). (f) Percentages of CD8⁺ TILs (CD3⁺CD8⁺) in the distant tumors analyzed by flow cytometry. Data are presented as mean \pm s.e.m. ($n = 4$). (g) Percentages of Gz-B positive CD8⁺ TILs (CD3⁺CD8⁺Gz-B⁺) in the distant tumors analyzed by flow cytometry. Data are presented as mean \pm s.e.m. ($n = 4$). (h) Representative immunofluorescence images showing CD3⁺ T cells infiltrated into the distant tumors. (i) IFN- γ levels in the distant tumors collected from mice at 5 days after different treatments. Data are presented as mean \pm s.e.m.

Figure 4. continued

($n = 4$). Statistical significance was calculated via one-way ANOVA with a Tukey posthoc test. * $P < 0.05$; ** $P < 0.01$; *** $P < 0.001$; **** $P < 0.0001$.

as the “distant tumor” without any treatment (Figure 4a). When the size of the primary tumor reached 50–75 mm³, BALB/c mice bearing bilateral CT26 tumors were divided into the following four groups: untreated, BetP-Gel (20 μ L, 0.05 M BetP per mouse), free α PDL1 (70 μ g per mouse), and α PDL1@BetP-Gel (20 μ L, 0.05 M BetP per mouse; 70 μ g α PDL1 per mouse). The size of both primary and distant tumors was monitored closely after different treatments. As expected, with the help of BetP-Gel to enable TME modulation, local retention, sustained and controlled release of α PDL1, the growth of the primary tumor was significantly inhibited (Figure 4b). More interestingly, the distant tumors in mice with their primary tumor treated with α PDL1@BetP-Gel were also obviously eliminated (Figure 4c,d).

To explain the mechanism of abscopal effect induced by local injection of α PDL1@BetP-Gel, different immune cells in distant tumors were investigated by flow cytometry. Interestingly, the number of TILs (CD3⁺) (Figure 4e) and CD8⁺ TILs (CD3⁺CD8⁺) (Figure 4f) in distant tumors showed obvious increase. Importantly, the expression of cytotoxic protein Gz-B in T cells in distant tumors also obviously increased, indicating that the released α PDL1 from hydrogel could reverse T cell exhaustion (Figure 4g and Figure S10). The infiltration of effective T cells was further confirmed by the immunofluorescence staining of CD3⁺ TIL cells and the secretion of IFN- γ in the distant tumor (Figure 4h,i). Taken together, these results indicated that the local injection of α PDL1@BetP-Gel could trigger systemic antitumor immune responses and promote effective T cell activation even in abscopal tumors, showing promise in inhibiting tumor metastases.

Thus, the syringeable shear-thinning anti-inflammatory hydrogel is self-assembled by mixing BetP, a clinic-approved steroid anti-inflammatory drug, and calcium ions via non-covalent interactions including intermolecular hydrogen bonds, hydrophobic interactions, as well as coordination between phosphate groups and calcium ions. Moreover, such nanofiber hydrogel could as a carrier-free delivery platform for effective delivery of ICB antibodies such as α PDL1 after local injection, realizing prolonged retention of encapsulated antibodies. The nanofiber hydrogels after local injection into the mouse could be gradually degraded to release BetP and encapsulated antibodies via competitive coordination interactions between BetP and phosphates in physiological condition.

Interestingly, such localized drug-based nanofiber hydrogel is able to boost strong antitumor immune responses. This hydrogel itself could reprogram the inflammation-related immunosuppressive TME by scavenging the chronic inflammation including attenuating inflammation-related NF- κ B signaling pathway and decreasing the expression levels of pro-inflammatory cytokines and MMP2. The reprogrammed inflammation-related TME is characterized with improved tumor infiltration of effective T lymphocytes and reduced percentage of immunosuppressive cells. On the other hand, this nanofiber hydrogel could serve as an effective reservoir to allow local and sustained release of α PDL1, avoiding the systemic toxicity of ICB. Moreover, the sustainably released α PDL1 could effectively reverse T cell exhaustion over a long period of time, activating T cell-mediated immune attack of

cancer cells, inhibiting the growth of both primary and distant abscopal tumors. As the synergistic outcome of the above mechanism, it has been demonstrated that the local injection of α PDL1@BetP-Gel could effectively inhibit the growth of primary and distant tumors in the CT26 tumor model.

The current technique and formulation hold great potential for clinical translation. An immunotherapeutic nanofiber hydrogel such as this is synthesized by a simple mix of clinically used steroid drugs, antibodies, and calcium ions. The hydrogel with shear-thinning ability permits its direct injection into the tissues with minimal invasiveness. Thus, considering its composition with all clinically approved components, the rather simple and easily scaled up formulation process, the minimally invasive method of administration, as well as local controlled delivery of α PDL1 with low systemic toxicity but systemic therapeutic responses, our strategy may indeed have great potential to treat advanced metastatic cancer in clinics.

■ ASSOCIATED CONTENT

SI Supporting Information

The Supporting Information is available free of charge at <https://pubs.acs.org/doi/10.1021/acs.nanolett.0c02684>.

Experimental section and Figures S1–S18 ([PDF](#))

Video of nanofiber hydrogel rapidly recovering (self-healing) after being injected from a syringe ([MP4](#))

■ AUTHOR INFORMATION

Corresponding Authors

Zhuang Liu – Institute of Functional Nano and Soft Materials (FUNSOM), Jiangsu Key Laboratory for Carbon-Based Functional Materials & Devices, Soochow University, Suzhou 215123, Jiangsu, P.R. China;  orcid.org/0000-0002-1629-1039; Email: zliu@suda.edu.cn

Qian Chen – Institute of Functional Nano and Soft Materials (FUNSOM), Jiangsu Key Laboratory for Carbon-Based Functional Materials & Devices, Soochow University, Suzhou 215123, Jiangsu, P.R. China;  orcid.org/0000-0002-1487-5479; Email: chenqian@suda.edu.cn

Authors

Muchao Chen – Institute of Functional Nano and Soft Materials (FUNSOM), Jiangsu Key Laboratory for Carbon-Based Functional Materials & Devices, Soochow University, Suzhou 215123, Jiangsu, P.R. China

Yanjun Tan – Institute of Functional Nano and Soft Materials (FUNSOM), Jiangsu Key Laboratory for Carbon-Based Functional Materials & Devices, Soochow University, Suzhou 215123, Jiangsu, P.R. China

Ziliang Dong – Institute of Functional Nano and Soft Materials (FUNSOM), Jiangsu Key Laboratory for Carbon-Based Functional Materials & Devices, Soochow University, Suzhou 215123, Jiangsu, P.R. China

Jiaqi Lu – Institute of Functional Nano and Soft Materials (FUNSOM), Jiangsu Key Laboratory for Carbon-Based Functional Materials & Devices, Soochow University, Suzhou 215123, Jiangsu, P.R. China

Xiao Han — Institute of Functional Nano and Soft Materials (FUNSOM), Jiangsu Key Laboratory for Carbon-Based Functional Materials & Devices, Soochow University, Suzhou 215123, Jiangsu, P.R. China

Qiutong Jin — Institute of Functional Nano and Soft Materials (FUNSOM), Jiangsu Key Laboratory for Carbon-Based Functional Materials & Devices, Soochow University, Suzhou 215123, Jiangsu, P.R. China

Wenjun Zhu — Institute of Functional Nano and Soft Materials (FUNSOM), Jiangsu Key Laboratory for Carbon-Based Functional Materials & Devices, Soochow University, Suzhou 215123, Jiangsu, P.R. China

Jingjing Shen — Institute of Functional Nano and Soft Materials (FUNSOM), Jiangsu Key Laboratory for Carbon-Based Functional Materials & Devices, Soochow University, Suzhou 215123, Jiangsu, P.R. China

Liang Cheng — Institute of Functional Nano and Soft Materials (FUNSOM), Jiangsu Key Laboratory for Carbon-Based Functional Materials & Devices, Soochow University, Suzhou 215123, Jiangsu, P.R. China; orcid.org/0000-0001-5324-9094

Complete contact information is available at:
<https://pubs.acs.org/10.1021/acs.nanolett.0c02684>

Author Contributions

Q.C., Z.L., and M.C. conceived and designed the experiments. M.C., Y.T., Z.D., L.C., J.L., Y.T., X.H., Q.J., W.J., and J.S. performed the experiments and analyzed data. Q.C. and M.C. cowrote the paper. All authors discussed the results and implications and edited the manuscript at all stages.

Notes

The authors declare no competing financial interest.

ACKNOWLEDGMENTS

This article was partially supported by the National Research Programs of China (2016YFA0201200), the National Natural Science Foundation of China (91959104, 21927803, 51903182, 51525203), the Natural Science Foundation of Jiangsu Province (BK20190826), Collaborative Innovation Center of Suzhou Nano Science and Technology, and the 111 Program from the Ministry of Education of China.

REFERENCES

- (1) Sharma, P.; Allison, J. P. The Future of Immune Checkpoint Therapy. *Science (Washington, DC, U. S.)* **2015**, *348* (6230), 56–61.
- (2) Topalian, S. L.; Taube, J. M.; Anders, R. A.; Pardoll, D. M. Mechanism-Driven Biomarkers to Guide Immune Checkpoint Blockade in Cancer Therapy. *Nat. Rev. Cancer* **2016**, *16* (5), 275–287.
- (3) Topalian, S. L.; Drake, C. G.; Pardoll, D. M. Immune Checkpoint Blockade: A Common Denominator Approach to Cancer Therapy. *Cancer Cell* **2015**, *27* (4), 450–461.
- (4) Teng, F.; Meng, X.; Kong, L.; Yu, J. Progress and Challenges of Predictive Biomarkers of Anti PD-1/PD-L1 Immunotherapy: A Systematic Review. *Cancer Lett.* **2018**, *414*, 166–173.
- (5) McGranahan, N.; Furness, A. J. S.; Rosenthal, R.; Ramskov, S.; Lyngaae, R.; Saimi, S. K.; Jamal-Hanjani, M.; Wilson, G. A.; Birkbak, N. J.; Hiley, C. T.; Watkins, T. B. K.; Shafit, S.; Murugaesu, N.; Mitter, R.; Akarca, A. U.; Linares, J.; Marafioti, T.; Henry, J. Y.; Van Allen, E. M.; Miao, D.; Schilling, B.; Schadendorf, D.; Garraway, L. A.; Makarov, V.; Rizvi, N. A.; Snyder, A.; Hellmann, M. D.; Mergenbauer, T.; Wolchok, J. D.; Shukla, S. A.; Wu, C. J.; Peggs, K. S.; Chan, T. A.; Hadrup, S. R.; Quezada, S. A.; Swanton, C. Clonal Neoantigens Elicit T Cell Immunoreactivity and Sensitivity to Immune Checkpoint Blockade. *Science (Washington, DC, U. S.)* **2016**, *351* (6280), 1463–1469.
- (6) Nishino, M.; Ramaiya, N. H.; Hatabu, H.; Hodin, F. S. Monitoring Immune-Checkpoint Blockade: Response Evaluation and Biomarker Development. *Nat. Rev. Clin. Oncol.* **2017**, *14* (11), 655–668.
- (7) Lindau, D.; Gielen, P.; Kroesen, M.; Wesseling, P.; Adema, G. J. The Immunosuppressive Tumour Network: Myeloid-Derived Suppressor Cells, Regulatory T Cells and Natural Killer T Cells. *Immunology* **2013**, *138* (2), 105–115.
- (8) Gabrilovich, D. I.; Ostrand-Rosenberg, S.; Bronte, V. Coordinated Regulation of Myeloid Cells by Tumours. *Nat. Rev. Immunol.* **2012**, *12* (4), 253–268.
- (9) Michot, J. M.; Bigenwald, C.; Champiat, S.; Collins, M.; Carbonnel, F.; Postel-Vinay, S.; Berdelou, A.; Varga, A.; Bahleda, R.; Hollebecque, A.; Massard, C.; Fuereia, A.; Ribrag, V.; Gazzah, A.; Armand, J. P.; Amellal, N.; Angevin, E.; Noel, N.; Boutros, C.; Mateus, C.; Robert, C.; Soria, J. C.; Marabelle, A.; Lambotte, O. Immune-Related Adverse Events with Immune Checkpoint Blockade: A Comprehensive Review. *Eur. J. Cancer* **2016**, *54*, 139–148.
- (10) de Velasco, G.; Bermas, B.; Choueiri, T. K. Autoimmune Arthropathy and Uveitis as Complications of Programmed Death 1 Inhibitor Treatment. *Arthritis Rheumatol.* **2016**, *68* (2), 556–557.
- (11) Postow, M. A.; Sidlow, R.; Hellmann, M. D. Immune-Related Adverse Events Associated with Immune Checkpoint Blockade. *N. Engl. J. Med.* **2018**, *378* (2), 158–168.
- (12) Joyce, J. A.; Fearon, D. T. T Cell Exclusion, Immune Privilege, and the Tumor Microenvironment. *Science (Washington, DC, U. S.)* **2015**, *348* (6230), 74–80.
- (13) Chen, Q.; Xu, L.; Chen, J.; Yang, Z.; Liang, C.; Yang, Y.; Liu, Z. Tumor Vasculature Normalization by Orally Fed Erlotinib to Modulate the Tumor Microenvironment for Enhanced Cancer Nanomedicine and Immunotherapy. *Biomaterials* **2017**, *148*, 69–80.
- (14) Saeed, M.; Gao, J.; Shi, Y.; Lammers, T.; Yu, H. Engineering Nanoparticles to Reprogram the Tumor Immune Microenvironment for Improved Cancer Immunotherapy. *Theranostics* **2019**, *9* (26), 7981–8000.
- (15) Balkwill, F.; Mantovani, A. Inflammation and Cancer: Back to Virchow? *Lancet* **2001**, *357* (9255), 539–545.
- (16) Park, M.; Hong, J. Roles of NF-KB in Cancer and Inflammatory Diseases and Their Therapeutic Approaches. *Cells* **2016**, *5* (2), 15.
- (17) Candido, J.; Hagemann, T. Cancer-Related Inflammation. *J. Clin. Immunol.* **2013**, *33* (S1), 79–84.
- (18) Galli, S. J.; Borregaard, N.; Wynn, T. A. Phenotypic and Functional Plasticity of Cells of Innate Immunity: Macrophages, Mast Cells and Neutrophils. *Nat. Immunol.* **2011**, *12* (11), 1035–1044.
- (19) Chen, Q.; Chen, G.; Chen, J.; Shen, J.; Zhang, X.; Wang, J.; Chan, A.; Gu, Z. Bioresponsive Protein Complex of APD1 and ACD47 Antibodies for Enhanced Immunotherapy. *Nano Lett.* **2019**, *19* (8), 4879–4889.
- (20) Coussens, L. M.; Zitvogel, L.; Palucka, A. K. Neutralizing Tumor-Promoting Chronic Inflammation: A Magic Bullet? *Science (Washington, DC, U. S.)* **2013**, *339* (6117), 286–291.
- (21) Zelenay, S.; Van Der Veen, A. G.; Böttcher, J. P.; Snelgrove, K. J.; Rogers, N.; Acton, S. E.; Chakravarty, P.; Girotti, M. R.; Marais, R.; Quezada, S. A.; Sahai, E.; Reis E Sousa, C. Cyclooxygenase-Dependent Tumor Growth through Evasion of Immunity. *Cell* **2015**, *162* (6), 1257–1270.
- (22) Erreni, M.; Mantovani, A.; Allavena, P. Tumor-Associated Macrophages (TAM) and Inflammation in Colorectal Cancer. *Cancer Microenviron.* **2011**, *4* (2), 141–154.
- (23) Mantovani, A.; Sica, A. Macrophages, Innate Immunity and Cancer: Balance, Tolerance, and Diversity. *Curr. Opin. Immunol.* **2010**, *22* (2), 231–237.
- (24) Quail, D. F.; Joyce, J. A. Microenvironmental Regulation of Tumor Progression and Metastasis. *Nat. Med.* **2013**, *19* (11), 1423–1437.
- (25) Oude Munnink, T.; Henstra, M.; Segerink, L.; Movig, K.; Brummelhuis-Visser, P. Therapeutic Drug Monitoring of Monoclonal

- Antibodies in Inflammatory and Malignant Disease: Translating TNF- α Experience to Oncology. *Clin. Pharmacol. Ther.* **2016**, *99* (4), 419–431.
- (26) Jiang, H.; Hegde, S.; DeNardo, D. G. Tumor-Associated Fibrosis as a Regulator of Tumor Immunity and Response to Immunotherapy. *Cancer Immunol. Immunother.* **2017**, *66* (8), 1037–1048.
- (27) Goswami, K. K.; Ghosh, T.; Ghosh, S.; Sarkar, M.; Bose, A.; Baral, R. Tumor Promoting Role of Anti-Tumor Macrophages in Tumor Microenvironment. *Cell. Immunol.* **2017**, *316*, 1–10.
- (28) Palucka, A. K.; Coussens, L. M. The Basis of Oncoimmunology. *Cell* **2016**, *164* (6), 1233–1247.
- (29) Li, J.; Mooney, D. J. Designing Hydrogels for Controlled Drug Delivery. *Nat. Rev. Mater.* **2016**, *1* (12), 16071.
- (30) Appel, E. A.; del Barrio, J.; Loh, X. J.; Scherman, O. A. Supramolecular Polymeric Hydrogels. *Chem. Soc. Rev.* **2012**, *41* (18), 6195.
- (31) Lei, K.; Tang, L. Surgery-Free Injectable Macroscale Biomaterials for Local Cancer Immunotherapy. *Biomater. Sci.* **2019**, *7* (3), 733–749.
- (32) Zhang, Y.; Ding, J.; Qi, B.; Tao, W.; Wang, J.; Zhao, C.; Peng, H.; Shi, J. Multifunctional Fibers to Shape Future Biomedical Devices. *Adv. Funct. Mater.* **2019**, *29* (34), 1902834.
- (33) Jin, H.; Wan, C.; Zou, Z.; Zhao, G.; Zhang, L.; Geng, Y.; Chen, T.; Huang, A.; Jiang, F.; Feng, J.-P.; Lovell, J. F.; Chen, J.; Wu, G.; Yang, K. Tumor Ablation and Therapeutic Immunity Induction by an Injectable Peptide Hydrogel. *ACS Nano* **2018**, *12* (4), 3295–3310.
- (34) Yu, S.; He, C.; Chen, X. Injectable Hydrogels as Unique Platforms for Local Chemotherapeutics-Based Combination Antitumor Therapy. *Macromol. Biosci.* **2018**, *18* (12), 1800240.
- (35) Dai, X.; Meng, J.; Deng, S.; Zhang, L.; Wan, C.; Lu, L.; Huang, J.; Hu, Y.; Zhang, Z.; Li, Y.; Lovell, J. F.; Wu, G.; Yang, K.; Jin, H. Targeting CAMKII to Reprogram Tumor-Associated Macrophages and Inhibit Tumor Cells for Cancer Immunotherapy with an Injectable Hybrid Peptide Hydrogel. *Theranostics* **2020**, *10* (7), 3049–3063.
- (36) Shi, Y.; Wang, Z.; Zhang, X.; Xu, T.; Ji, S.; Ding, D.; Yang, Z.; Wang, L. Multi-Responsive Supramolecular Hydrogels for Drug Delivery. *Chem. Commun.* **2015**, *51* (83), 15265–15267.
- (37) Cheetham, A. G.; Zhang, P.; Lin, Y.; Lock, L. L.; Cui, H. Supramolecular Nanostructures Formed by Anticancer Drug Assembly. *J. Am. Chem. Soc.* **2013**, *135* (8), 2907–2910.
- (38) Liu, Q.; Zhan, C.; Barhoumi, A.; Wang, W.; Santamaría, C.; McAlvin, J. B.; Kohane, D. S. A Supramolecular Shear-Thinning Anti-Inflammatory Steroid Hydrogel. *Adv. Mater.* **2016**, *28* (31), 6680–6686.
- (39) Criswell, S. M.; Balkwill, F. R. Inflammation and Cancer: Advances and New Agents. *Nat. Rev. Clin. Oncol.* **2015**, *12* (10), 584–596.
- (40) Hetland, M. L.; Østergaard, M.; Ejbjerg, B.; Jacobsen, S.; Stengaard-Pedersen, K.; Junker, P.; Lottenburger, T.; Hansen, I.; Andersen, L. S.; Tarp, U.; Svendsen, A.; Pedersen, J. K.; Skjødt, H.; Ellingsen, T.; Lindegaard, H.; Pødenphant, J.; Hørslev-Petersen, K. Short- and Long-Term Efficacy of Intra-Articular Injections with Betamethasone as Part of a Treat-to-Target Strategy in Early Rheumatoid Arthritis: Impact of Joint Area, Repeated Injections, MRI Findings, Anti-CCP, IgM-RF and CRP. *Ann. Rheum. Dis.* **2012**, *71* (6), 851–856.
- (41) Qiao, Y.; Lin, Y.; Yang, Z.; Chen, H.; Zhang, S.; Yan, Y.; Huang, J. Unique Temperature-Dependent Supramolecular Self-Assembly: From Hierarchical 1D Nanostructures to Super Hydrogel. *J. Phys. Chem. B* **2010**, *114* (36), 11725–11730.
- (42) Chakrabarty, A.; Maitra, U.; Das, A. D. Metal Cholate Hydrogels: Versatile Supramolecular Systems for Nanoparticle Embedded Soft Hybrid Materials. *J. Mater. Chem.* **2012**, *22* (35), 18268–18274.
- (43) Jia, Y.-G.; Zhu, X. X. Self-Healing Supramolecular Hydrogel Made of Polymers Bearing Cholic Acid and β -Cyclodextrin Pendants. *Chem. Mater.* **2015**, *27* (1), 387–393.
- (44) Grivennikov, S. I.; Greten, F. R.; Karin, M. Immunity, Inflammation, and Cancer. *Cell* **2010**, *140* (6), 883–899.
- (45) Luo, J. L.; Maeda, S.; Hsu, L. C.; Yagita, H.; Karin, M. Inhibition of NF-KB in Cancer Cells Converts Inflammation-Induced Tumor Growth Mediated by TNF α to TRAIL-Mediated Tumor Regression. *Cancer Cell* **2004**, *6* (3), 297–305.
- (46) Zulfakar, M. H.; Abdelouahab, N.; Heard, C. M. Enhanced Topical Delivery and Ex Vivo Anti-Inflammatory Activity from a Betamethasone Dipropionate Formulation Containing Fish Oil. *Inflammation Res.* **2010**, *59* (1), 23–30.
- (47) Stahn, C.; Löwenberg, M.; Hommes, D. W.; Buttigereit, F. Molecular Mechanisms of Glucocorticoid Action and Selective Glucocorticoid Receptor Agonists. *Mol. Cell. Endocrinol.* **2007**, *275* (1–2), 71–78.
- (48) Cain, D. W.; Cidlowski, J. A. Immune Regulation by Glucocorticoids. *Nat. Rev. Immunol.* **2017**, *17* (4), 233–247.
- (49) Koyama, S.; Akbay, E. A.; Li, Y. Y.; Aref, A. R.; Skoulidis, F.; Herter-Sprie, G. S.; Buczkowski, K. A.; Liu, Y.; Awad, M. M.; Denning, W. L.; Diao, L.; Wang, J.; Parra-Cuentas, E. R.; Wistuba, I. I.; Soucheray, M.; Thai, T.; Asahina, H.; Kitajima, S.; Altabef, A.; Cavanaugh, J. D.; Rhee, K.; Gao, P.; Zhang, H.; Fecci, P. E.; Shimamura, T.; Hellmann, M. D.; Heymach, J. V.; Hodis, F. S.; Freeman, G. J.; Barbie, D. A.; Dranoff, G.; Hammerman, P. S.; Wong, K.-K. STK11/LKB1 Deficiency Promotes Neutrophil Recruitment and Proinflammatory Cytokine Production to Suppress T-Cell Activity in the Lung Tumor Microenvironment. *Cancer Res.* **2016**, *76* (5), 999–1008.
- (50) Garris, C. S.; Arlauckas, S. P.; Kohler, R. H.; Trefny, M. P.; Garren, S.; Piot, C.; Engblom, C.; Pfirsichke, C.; Siwicki, M.; Gungabeesoon, J.; Freeman, G. J.; Warren, S. E.; Ong, S.; Browning, E.; Twitty, C. G.; Pierce, R. H.; Le, M. H.; Algazi, A. P.; Daud, A. I.; Pai, S. I.; Zippelius, A.; Weissleder, R.; Pittet, M. J. Successful Anti-PD-1 Cancer Immunotherapy Requires T Cell-Dendritic Cell Crosstalk Involving the Cytokines IFN- γ and IL-12. *Immunity* **2018**, *49* (6), 1148–1161.
- (51) Huang, D.; Chen, J.; Yang, L.; Ouyang, Q.; Li, J.; Lao, L.; Zhao, J.; Liu, J.; Lu, Y.; Xing, Y.; Chen, F.; Su, F.; Yao, H.; Liu, Q.; Su, S.; Song, E. NKILA LncRNA Promotes Tumor Immune Evasion by Sensitizing T Cells to Activation-Induced Cell Death. *Nat. Immunol.* **2018**, *19* (10), 1112–1125.
- (52) Grinberg-Bleyer, Y.; Oh, H.; Desrichard, A.; Bhatt, D. M.; Caron, R.; Chan, T. A.; Schmid, R. M.; Klein, U.; Hayden, M. S.; Ghosh, S. NF-KB c-Rel Is Crucial for the Regulatory T Cell Immune Checkpoint in Cancer. *Cell* **2017**, *170* (6), 1096–1108.
- (53) Xiao, Z.; Su, Z.; Han, S.; Huang, J.; Lin, L.; Shuai, X. Dual PH-Sensitive Nanodrug Blocks PD-1 Immune Checkpoint and Uses T Cells to Deliver NF-KB Inhibitor for Antitumor Immunotherapy. *Sci. Adv.* **2020**, *6* (6), no. eaay7785.
- (54) Gonzalez-Gugel, E.; Saxena, M.; Bhardwaj, N. Modulation of Innate Immunity in the Tumor Microenvironment. *Cancer Immunol. Immunother.* **2016**, *65* (10), 1261–1268.
- (55) Bor-Ching, S.; Su-Ming, H.; Hong-Nerg, H.; Huang-Chun, L.; Su-}Cheng, H.; Rong-Hwa, L. A Novel Role of Metalloproteinase in Cancer-Mediated Immunosuppression. *Cancer Res.* **2001**, *61*, 237–242.
- (56) Piromkraipak, P.; Sangpairoj, K.; Tirakotai, W.; Chaithirayanon, K.; Unchern, S.; Supavilai, P.; Power, C.; Vivithanaporn, P. Cysteinyl Leukotriene Receptor Antagonists Inhibit Migration, Invasion, and Expression of MMP-2/9 in Human Glioblastoma. *Cell. Mol. Neurobiol.* **2018**, *38* (2), 559–573.
- (57) Bauvois, B. New Facets of Matrix Metalloproteinases MMP-2 and MMP-9 as Cell Surface Transducers: Outside-in Signaling and Relationship to Tumor Progression. *Biochim. Biophys. Acta, Rev. Cancer* **2012**, *1825* (1), 29–36.
- (58) Godefroy, E.; Manches, O.; Dréno, B.; Hochman, T.; Rolnitzky, L.; Labarrière, N.; Guilloux, Y.; Goldberg, J.; Jotereau, F.; Bhardwaj, N. Matrix Metalloproteinase-2 Conditions Human Dendritic Cells to Prime Inflammatory TH2 Cells via an IL-12- and OX40L-Dependent Pathway. *Cancer Cell* **2011**, *19* (3), 333–346.

- (59) Becker, J. C.; Andersen, M. H.; Schrama, D.; Thor Straten, P. Immune-Suppressive Properties of the Tumor Microenvironment. *Cancer Immunol. Immunother.* **2013**, *62* (7), 1137–1148.